Contribution of the excitation of conduction band electrons to the kinetic electron emission induced by slow ions in metals

J. I. Juaristi
Departamento de Física de Materiales, Facultad de Químicas, Universidad del País Vasco, Apartado 1072, 20080 Donostia, Spain

M. Rösler
Hahn-Meitner Institute Berlin, Bereich FD, Glienicker Strasse 100, D-14109 Berlin, Germany

F. J. García de Abajo
Departamento de Ciencias de la Computación e Inteligencia Artificial, Facultad de Informatica, Universidad del País Vasco, Apartado 649, 20080 Donostia, Spain

(Received 21 April 1998)

A model is presented to calculate the energy and angle distribution of excited conduction band electrons in binary collisions with slowly moving ions. The scattering of the conduction band electrons, which are described within the free electron model, off the effective potential created by the projectile is studied, taking into account the shift of the Fermi sphere due to the nonzero velocity of the ion. The effective potential is calculated self-consistently within the density functional theory for a static impurity embedded in an electron gas. Using the excitation rate of conduction band electrons obtained from this approach, the total electron yield of emitted electrons is calculated within a transport equation formalism. The obtained results are compared to experimental data. [S0163-1829(98)03247-0]

I. INTRODUCTION

The study of electron emission induced by incident ions in metals is a valuable tool to analyze the properties and structure of both projectile and target material. Two different types of electron emission are distinguished depending on the origin of the excitation energy of the emitted electrons.

In potential emission this energy comes from the potential energy of the projectile. This emission mechanism is due to Auger transitions, in which a target electron is excited by the energy liberated in the capture of an electron in a state bound to the projectile.[1]

In the kinetic electron emission the electron excitation energy comes from the kinetic energy of the projectile. This means that kinetic electron emission is accompanied by slowing down of the projectile, i.e., electron excitation mechanisms that give rise to kinetic electron emission constitute the electronic stopping power of the target with respect to the incident ion. Using this, frequently applied theoretical methods[2,3] consider the total number of emitted kinetic electrons (the total yield) to be proportional to the electronic stopping power.

It is the aim of this work to go beyond this approximation and to obtain from a free parameter model absolute values of the kinetic emission yield. In Sec. II of this paper, a model is presented to calculate the excitation of conduction band electrons of a metal induced by slowly moving ions ($v < v_F$, where v_F is the Fermi velocity of the conduction band electrons and v is the velocity of the projectile). Since the perturbation that a slow ion represents to the valence band electrons is very strong, linear theory is not expected to be valid[4] to calculate electron excitation spectra.[5] Therefore, the induced potential created by the ion is calculated self-consistently and the scattering of the electrons by this potential is calculated to all orders in Z_1 the atomic number of the projectile, taking into account the shift of the Fermi sphere due to the nonzero velocity of the ion. This model is based on a model first proposed and developed by Calera-Rubio *et al.*,[6,7] in which they did not take into account the shift of the Fermi sphere. Then, the transport and escape of the electrons through the surface potential barrier is calculated using a model based on the solution of the Boltzmann transport equation.

In Sec. III, our model results are compared to experimental data. The effect of the elastic scattering suffered by the excited electrons with the target atoms is discussed. Finally, Sec. IV is devoted to the conclusions of this work. Atomic units (a.u.) will be used unless it is otherwise stated.

II. THEORY

A. Model for excitation

1. Kinematic constrains

When a slowly moving ion travels through a free electron gas it excites electron-hole pairs, i.e., some electrons are scattered by the potential created by the projectile from occupied electronic states below the Fermi energy, to unoccupied states above the Fermi energy. From now on, the free electron states are characterized in the laboratory system (lab) by their wave vector $\mathbf{k}$, with polar angle θ (the angle between the direction of $\mathbf{k}$ and $\mathbf{v}$ the velocity of the ion) and the azimuthal angle φ. In the center of mass (c.m.) system, in which the ion can be considered to be at rest, as the ionic mass is much larger than the electronic mass, the electronic states are described by the wave vector $\mathbf{k}'$, where $\mathbf{k}' = \mathbf{k} - \mathbf{v}$.

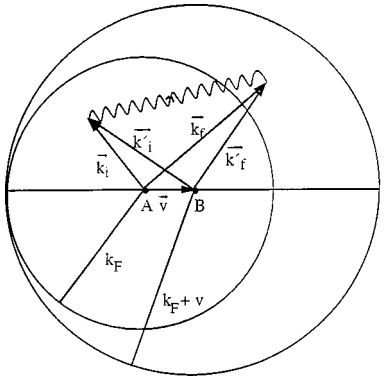

FIG. 1. Schematic representation in momentum space of the electronic excitations induced by a slow ion ($v<v_F$) traveling through a free electron gas. The sphere centered at point A is the Fermi sphere of initially occupied states. Point B, which is shifted from A by the velocity of the ion v, is the origin of momentum in the c.m. system. The electronic transitions that take place are those from initial states inside the Fermi sphere ($k_i<k_F$) to final states outside the Fermi sphere ($k_f>k_F$), such that the energy of the initial and final states is the same in the c.m. system ($k'_i=k'_f$). This implies that the sphere of radius k_F+v centered at B limits the maximum energy of the available final states.

The transition probabilities from occupied $\mathbf{k}_i$ ($k_i<k_F$) states to unoccupied $\mathbf{k}_f$ ($k_f>k_F$) states, where k_F is the Fermi wave vector, must be evaluated in order to obtain the electronic excitation spectrum (in atomic units $k_F=v_F$). Since the recoil of the ion is negligible, energy conservation law only allows transitions between equienergetic states in the c.m. system: $k'_i=k'_f$, and since $k_i<k_F$, the inequality $k_F-v\leqslant k'_i=k'_f\leqslant k_F+v$ is obtained.

Now, we are able to calculate the modulus of the (lab) wave vector of the most energetic excited electrons:

$$k_{f,\max}=k'_{f,\max}+v=k'_{i,\max}+v=k_{i,\max}+v+v=k_F+2v. \tag{1}$$

Therefore, the maximum energy, measured from the Fermi level that an electron can have after a single collision with the projectile is

$$\varepsilon_{\max}=\frac{1}{2}\,(k^2_{f,\max}-k^2_F)=2v(k_F+v). \tag{2}$$

The electronic excitations that take place are described in Fig. 1. In this figure two different spheres are represented. The one centered at point A is the Fermi sphere of radius k_F, and it encloses the electronic states that are occupied before the interaction with the projectile takes place, i.e., the initial states of the transitions. The second sphere is centered at point B, which is shifted by the velocity of the ion v ($v<k_F$) from point A. Point B is the origin of momenta in the c.m. system. The radius of this sphere is k_F+v, and the volume that it encloses, outside the Fermi sphere, corresponds to the available final electronic states after the interaction with the projectile. An electron in an initial state $k_i<k_F$ inside the Fermi sphere may be scattered into a final state $k_f>k_F$ outside the Fermi sphere, if the modulus of the wave vector of both states measured in the c.m. system is equal, i.e., if the distances from point B $k'_i=|\mathbf{k}_i-\mathbf{v}|$ and $k'_f=|\mathbf{k}_f-\mathbf{v}|$ are the same. Therefore, the same value of k', the modulus of the wave vector in the c.m. system, may correspond to initially occupied or unoccupied states depending on θ', the angle between the wave vector in the c.m. system and the direction of the velocity of the ion v. More precisely, if the state is an initially occupied $\mathbf{k}_i$ state inside the Fermi sphere

$$\cos(\theta'_i)<\frac{k_F^2-k_i'^2-v^2}{2vk'_i} \tag{3a}$$

and if it is an initially unoccupied $\mathbf{k}_f$ state outside the Fermi sphere

$$\cos(\theta'_f)>\frac{k_F^2-k_f'^2-v^2}{2vk'_f}. \tag{3b}$$

2. Transition probabilities and electronic excitation spectra

The probability for exciting an electron from the state $\mathbf{k}'_i$ to the state $\mathbf{k}'_f$ is calculated using the following expression:

$$\tilde{\omega}(\mathbf{k}'_i,\mathbf{k}'_f)=2\pi|T_{if}|^2\delta(\varepsilon'_i-\varepsilon'_f), \tag{4}$$

where T_{if} is the transition matrix element between the states $\mathbf{k}'_i$ and $\mathbf{k}'_f$, and the δ function ensures conservation of energy. T_{if} can be calculated as a function of the differential scattering cross section[8] $\sigma(\beta)$

$$|T_{if}|^2=4\pi^2\sigma(\beta), \tag{5}$$

where β is the angle between $\mathbf{k}'_i$ and $\mathbf{k}'_f$

$$\cos(\beta)=\cos(\theta'_i)\cos(\theta'_f)+\sin(\theta'_i)\sin(\theta'_f)\cos(\varphi'_i-\varphi'_f) \tag{6}$$

The quantity $\omega\,(\varepsilon'_i,\varepsilon'_f,\Omega'_i,\Omega'_f)$ is defined as the probability for exciting an electron from the state with energy ε'_i with wave vector in the direction of the solid angle Ω'_i (θ'_i,φ'_i) to the state with energy ε'_f with wave vector in the direction of the solid angle Ω'_f (θ'_f,φ'_f). Using Eq. (4),

$$\rho(\varepsilon'_i)\rho(\varepsilon'_f)\omega(\varepsilon'_i,\varepsilon'_f,\Omega'_i,\Omega'_f)d\varepsilon'_i d\varepsilon'_f d\Omega'_i d\Omega'_f$$
$$=\frac{1}{2}\,\tilde{\omega}(\mathbf{k}'_i,\mathbf{k}'_f)d^3\mathbf{k}'_i d^3\mathbf{k}'_f. \tag{7}$$

The $\frac{1}{2}$ factor at the right-hand side of Eq. (7) appears because the electron spin does not change during the excitation, and $\rho(\varepsilon'_i)$ is the density of states with energy ε':

$$\rho(\varepsilon')=\frac{\sqrt{2\varepsilon'}}{\pi^2}. \tag{8}$$

In this way, the following expression for $\omega(\varepsilon'_i,\varepsilon'_f,\Omega'_i,\Omega'_f)$ is obtained:

$$\omega(\varepsilon'_i,\varepsilon'_f,\Omega'_i,\Omega'_f)=\frac{1}{2}\,\frac{1}{16\pi^2}\,\tilde{\omega}(\mathbf{k}'_i,\mathbf{k}'_f)$$
$$=\frac{\pi}{4}\,\sigma(\beta)\,\delta(\varepsilon'_i-\varepsilon'_f). \tag{9}$$

The integration of expression (9) over the initial states gives $P(\varepsilon_f',\Omega_f')$, the probability of creating an excitation with energy ε_f' in the direction given by the solid angle Ω_f':

$$P(\varepsilon_f',\Omega_f')=\int_{\varepsilon'_{\min}}^{\varepsilon'_{\max}} d\varepsilon_i'\,\rho(\varepsilon_i')\int_{\theta'_{\min}}^{\pi} d\theta_i' \times\sin\theta_i'\int_0^{2\pi} d\varphi_i'\,\omega(\varepsilon_i',\varepsilon_f',\Omega_i',\Omega_f'), \quad (10)$$

where $\varepsilon'_{\min}=\frac{1}{2}(k_F-v)^2$, $\varepsilon'_{\max}=\frac{1}{2}(k_F+v)^2$, and $\theta'_{\min}$ is obtained from Eq. (3a). The integration in energies is performed making use of the δ function:

$$P(\varepsilon_f',\Omega_f')=\frac{\pi\rho(\varepsilon_f')}{4}\int_{\theta'_{\min}}^{\pi} d\theta_i'\sin\theta_i'\int_0^{2\pi} d\varphi_i'\,\sigma(\beta). \quad (11)$$

In order to calculate $\sigma(\beta)$ the effective potential created by the moving ion inside the electron gas is needed. This potential is not spherically symmetric. Nevertheless, for the low velocities under consideration, we assume that it is a good approximation to use, instead of the dynamic potential, the spherically symmetric static potential.[9] The effective static potential is calculated self-consistently using the density functional formalism[10,11] (DFT) for the case of a static impurity embedded in an electron gas.[12] For a spherically symmetric scattering potential the differential scattering cross section can be calculated as a function of the scattering phase shifts in the following way:[13]

$$\sigma(\beta)=\frac{1}{k_f'^2}\left|\sum_{l=0}^{\infty}(2l+1)e^{i\delta_l(k_f')}\sin[\delta_l(k_f')]P_l(\cos\beta)\right|^2, \quad (12)$$

where the P_1-s are the Legendre Polynomials and $\delta_1(k_f')$ are the scattering phase shifts at the considered energy. The squared expression in Eq. (12) can be expanded in the following way:

$$\left|\sum_{l=0}^{\infty}(2l+1)e^{i\delta_l(k_f')}\sin[\delta_l(k_f')]P_l(\cos\beta)\right|^2 =\sum_{l=0}^{\infty}\sum_{l'=0}^{\infty}A[\delta_l(k_f'),\delta_{l'}(k_f')] \times(2l+1)(2l'+1)P_l(\cos\beta)P_{l'}(\cos\beta), \quad (13)$$

where

$$A(\delta_l,\delta_{l'})=\sin(\delta_l)\sin(\delta_{l'})\cos(\delta_l-\delta_{l'}). \quad (14)$$

Making use of Eqs. (12) and (13) and integrating Eq. (11) over its azimuthal dependence, the probability of exciting an electron to the state with energy ε_f' and with an angle θ_f' between its velocity and the velocity of the ion is obtained

$$P(\varepsilon_f',\theta_f')=\frac{1}{2\sqrt{2\varepsilon_f'}}\sum_{l=0}^{\infty}\sum_{l'=0}^{\infty}A[\delta_l(k_f'),\delta_{l'}(k_f')]B_{ll'}(\theta_f'), \quad (15a)$$

where

$$B_{ll'}(\theta_f')=(2l+1)(2l'+1)\int_{\theta'_{\min}}^{\pi} d\theta_i' \times\sin\theta_i'\int_0^{2\pi} d\varphi_i'\,P_l(\cos\beta)P_{l'}(\cos\beta) \quad (15b)$$

The number of electrons excited per unit time with energy ε_f' and angle θ_f', $Q(\varepsilon_f',\theta_f')$, is calculated in the following way:

$$Q(\varepsilon_f',\theta_f')=\rho(\varepsilon_f')P(\varepsilon_f',\theta_f')=\frac{\sqrt{2\varepsilon_f'}}{\pi^2}P(\varepsilon_f',\theta_f'). \quad (16)$$

We want to obtain this quantity in the lab system. Using the relations between the quantities measured in the c.m. and lab systems

$$\varepsilon'=\varepsilon+\tfrac{1}{2}v^2-v\sqrt{2\varepsilon}\cos\theta \quad (17a)$$

and

$$\theta'=\arctan\left(\frac{\sqrt{2\varepsilon}\sin\theta}{\sqrt{2\varepsilon}\cos\theta-v}\right) \quad (17b)$$

the number of excited electrons per unit time with energy ε and angle θ reads

$$Q(\varepsilon,\theta)=\rho[\varepsilon'(\varepsilon,\theta)]P[\varepsilon'(\varepsilon,\theta),\theta'(\varepsilon,\theta)] \times\frac{\sqrt{2\varepsilon}}{\sqrt{2\varepsilon-2\sqrt{2\varepsilon}\cos\theta}}. \quad (18)$$

Integration of this equation over the final energies gives the angular distribution of the electrons excited per unit time, meanwhile integration over final angles gives the energy distribution. More precisely

$$\frac{d^2N}{d(\cos\theta)dt}=\int_{E_F}^{E_F+2v(v+k_F)}Q(\varepsilon,\theta)d\varepsilon \quad (19)$$

and

$$\frac{d^2N}{d\varepsilon dt}=\int_0^{\pi}Q(\varepsilon,\theta)\sin\theta d\theta. \quad (20)$$

3. Stopping power

The formalism developed in the preceding section can also be used to calculate the stopping power of the ion. This is done making the product of the energy loss produced in the excitation of an electron from an initial state inside the Fermi sphere to a final state outside the Fermi sphere, with the probability per unit path of the ion of creating such excitation, and integrating it over all possible excitations:

$$\frac{dE}{dx}=\frac{1}{v}\int_{\varepsilon'_{\min}}^{\varepsilon'_{\max}}d\varepsilon'_f\rho(\varepsilon'_f)\int_0^{\theta'_{\max}}d\theta'_f\,\sin\theta'_f\int_0^{2\pi}d\varphi'_f \times\int_0^{2\pi}d\varphi'_i\int_{\theta'_{\min}}^{\pi}d\theta'_i\,\sin\theta'_i\int_{\varepsilon'_{\min}}^{\varepsilon'_{\max}} \times d\varepsilon'_i\rho(\varepsilon'_i)\omega(\varepsilon'_i,\varepsilon'_f,\Omega'_i,\Omega'_f)(\varepsilon_f-\varepsilon_i), \quad (21)$$

where $\varepsilon'_{\min}$ and $\varepsilon'_{\max}$ are the same as in Eq. (10) and $\theta'_{\min}$ and $\theta'_{\max}$ are obtained from Eqs. (3a) and (3b). Using Eq. (17a) we get the following relation:

$$\varepsilon_f-\varepsilon_i=\varepsilon'_f-\varepsilon'_i+v(\sqrt{2\varepsilon'_f}\cos\theta'_f-\sqrt{2\varepsilon'_i}\cos\theta'_i). \quad (22)$$

Finally, making use of Eqs. (9), (12), (13), and (22) the stopping power can be calculated in the following way:

$$\frac{dE}{dx}=\frac{1}{\sqrt{2}\pi^2}\int_{\varepsilon'_{\min}}^{\varepsilon'_{\max}}d\varepsilon'_f\sqrt{\varepsilon'_f}\int_0^{\theta'_{\max}}d\theta'_f\sin\theta'_f \times\sum_{l=0}^{\infty}\sum_{l'=0}^{\infty}\{A[\delta_l(\varepsilon'_f),\delta_{l'}(\varepsilon'_f)]C_{ll'}(\theta'_f)\}, \quad (23a)$$

where

$$C_{ll'}(\theta'_f)=(2l+1)(2l'+1)\int_{\theta'_{\min}}^{\pi}d\theta'_i\sin\theta'_i(\cos\theta'_f-\cos\theta'_i) \times\int_0^{2\pi}d\varphi'_i P_l(\cos\beta)P_{l'}(\cos\beta). \quad (23b)$$

4. Low-velocity limit

A similar model was presented by Calera-Rubio *et al.*[6] but without taking into account the shift of the Fermi sphere due to the non zero velocity of the ion. So they take the limit $v\to 0$, and analyze the case in which the lab and c.m. systems coincide. In this limit, taking into account the energy conservation law ($\varepsilon'_i=\varepsilon'_f$) Eq. (22) becomes

$$\varepsilon_f-\varepsilon_i=vk_F(\cos\theta_f-\cos\theta_i), \quad (24)$$

where $\sqrt{2\varepsilon'_f}=k_F$ (only electrons at the Fermi level are scattered) and $\theta'=\theta$ (lab and c.m. systems coincide). Now Eq. (9) becomes

$$\omega(\varepsilon_i,\varepsilon_f,\Omega_i,\Omega_f)=\frac{\pi}{4}\sigma(\beta)\delta[\varepsilon_f-\varepsilon_i +vk_F(\cos\theta_i-\cos\theta_f)]. \quad (25)$$

Performing the same integrations as before, and taking into account that all magnitudes are already measured in the lab system, the angle and energy distribution of excited electrons is obtained in the limit $v\to 0$.

Using this model, it is also possible to obtain the stopping power of the ion.[14] The result is the expression for the stopping power in the limit of low velocities:[15]

$$\frac{dE}{dx}=n_0 v v_F\sigma_{\rm tr}(v_F), \quad (26)$$

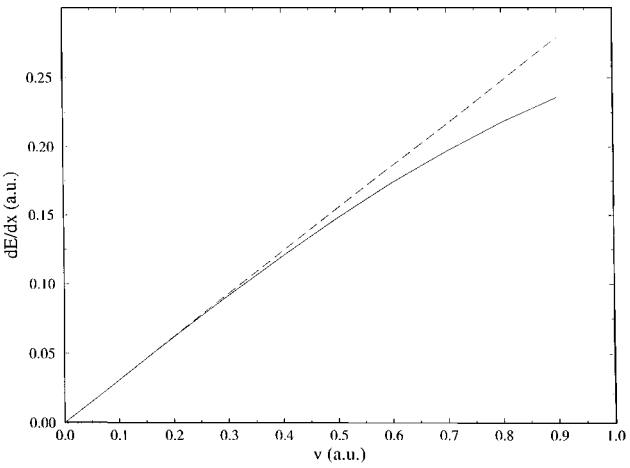

FIG. 2. Stopping power of a hydrogen atom traveling through a free electron gas with $r_s=1.5$ a.u., as a function of the velocity of the projectile. The solid line is obtained taking into account the shift of the Fermi sphere using Eq. (23). The dashed line represents the results obtained without taking the shift of the Fermi sphere into account making use of Eq. (26).

where n_0 is the electronic density of the conduction band of the metal and $\sigma_{\rm tr}(v_F)$ is the transport cross section at the Fermi energy. This equation is known to give good agreement with experimental results up to the Fermi velocity.[16,17,18] This fact has been theoretically justified in Ref. 19.

In Fig. 2 we present the results obtained for the stopping power of a hydrogen atom moving inside a free electron gas, which electronic density is given by $r_s=1.5$ a.u. ($r_s=\sqrt[3]{3/4\pi n_0}$) as a function of the velocity of the projectile. The results obtained using Eqs. (23) and (26) are compared. The negative curvature observed at high velocities when Eq. (23) is used, is the result of performing an exact calculation of the scattering but using the static potential instead of the stronger dynamic potential.[19] This is the reason why we expect that for velocities close to the Fermi velocity of the metal, this model will underestimate the stopping power and the total number of excited electrons. Nevertheless, the results obtained with both models are always similar and almost identical at low projectile velocities.

On the other hand, important differences exist between the results obtained with both models for the energy distributions of excited electrons. In Figs. (3a) and (3b) the comparison between the results obtained with both models for the energy distributions of the electrons excited per unit time $d^2N/d\varepsilon dt$ when a helium atom travels with velocities $v=0.4$ a.u. and $v=0.7$ a.u. through an electron gas is presented. In Fig. 3(a) $r_s=1.5$ a.u. is taken and in Fig. 3(b) $r_s=2.2$ a.u. The electron energy is measured from the Fermi level. It is observed that the model presented here gives a larger number of excited electrons at high energies and a smaller number of excited electrons at low energies than the model of Ref. 6. This is related to the fact that in our model the maximum energy an electron can gain in a collision with the projectile is $2v(v+v_F)$ while in the model of Ref. 6, strictly valid in the limit $v\to 0$, the value of this maximum energy is $2vv_F$. Since the electrons excited below the work function of the metal cannot escape from the solid and

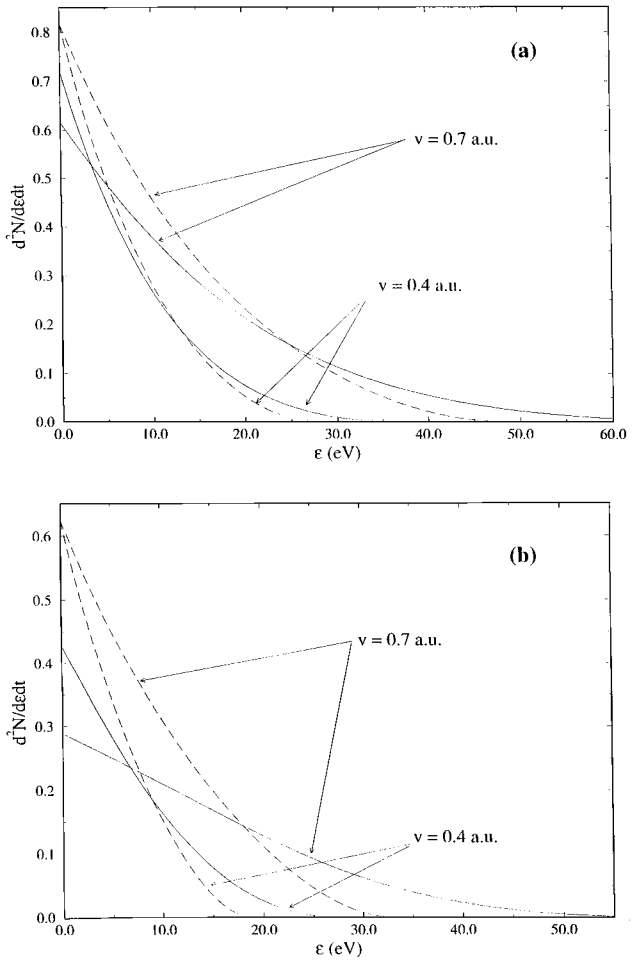

FIG. 3. Energy distributions of the electrons excited per unit time when a helium atom travels through a free electron gas. Results for projectile velocities $v=0.4$ a.u. and $v=0.7$ a.u. are presented. The solid line is obtained using the model presented in this work, i.e., taking into account the shift of the Fermi sphere. The dashed line is obtained using the model of Ref. 6. In (a) a value of $r_s=1.5$ a.u. has been taken, and in (b) $r_s=2.2$ a.u.

the $v\rightarrow 0$ approximation overestimates the number of excited low energy electrons, it is expected to give a smaller number of emitted electrons than our model. This effect is more important for high velocities, as the difference between the maximum excitation energies given by the two models increases with velocity as $2v^2$. Comparison between Figs. (3a) and (3b) shows that for the same velocity of the projectile the effect is more important the lower the electronic density of the metal is. This can be easily understood, since low electronic densities correspond to low Fermi velocities of the metal electrons, and the kinematic effects resulting from the shift of the Fermi sphere are more important for high relative values of the projectile velocity to the velocity of the electrons of the metal.

B. Transport model

The emission characteristics are determined by the density of inner excited electrons at the surface $N(\varepsilon,\Omega)$. This quantity is calculated in this work using the formalism developed in Ref. 20. Starting from the basic assumption of a homogeneous excitation inside the target, the transport equation can be written as

$$\frac{v_e(\varepsilon)}{l(\varepsilon)}N(\varepsilon,\Omega)=S(v;\varepsilon,\Omega)+\int_{\varepsilon}^{\infty}d\varepsilon'\times\int d\Omega' W(\varepsilon,\Omega,\varepsilon',\Omega')N(\varepsilon',\Omega'), \tag{27}$$

where $v_e(\varepsilon)$ and $l(\varepsilon)$ are the velocity and total mean free path (MFP) of the electron. The second term on the right-hand side denotes the number of electrons scattered into the state $\mathbf{k}(\varepsilon,\Omega)$ by collisions within the target. This number is expressed in terms of the transition function $W(\varepsilon,\Omega,\varepsilon',\Omega')$. The contribution of electrons created in the state $\mathbf{k}$ by the moving ion is described by the excitation function $S(v;\varepsilon,\Omega)$. With the energy and angle distribution of electrons excited per unit time $Q(\varepsilon,\theta)$ discussed in previous section, the excitation function can be written in the variables used in Eq. (27):

$$S(v;\varepsilon,\Omega)=\frac{1}{2\pi v}Q(\varepsilon,\theta). \tag{28}$$

The total MFP as well as the transition functions are determined by inelastic and elastic processes. The inelastic scattering properties given in Ref. 20 are calculated in random phase approximation for an electron gas.[21]

The escape process is described by the model of a planar surface barrier and free electrons inside the metal using the conservation laws for energy and parallel momentum of the electrons. Measurable quantities as the energy spectra of emerging electrons and the yield can be obtained in a simple way from the solution of the transport equation.

III. RESULTS

A. Effect of elastic scattering

In Fig. 4 the inelastic, elastic, and total mean free paths of electrons in Au are presented as a function of the electron energy measured from the Fermi level. The elastic scattering properties are calculated by the partial wave method, using the phase shifts provided by Heinz[22] that are obtained using a muffin tin approximation with a suitable choice of the energy zero in the region between the muffin tin spheres, taking the correct lattice structure of Au into account. In order to calculate both the electron excitation spectra and the inelastic scattering properties of the electrons, a value of $r_s=1.5$ a.u. is chosen to characterize the electronic density of the conduction band of Au, which is obtained from the experimental value of the bulk plasmon energy.[23,24] In Fig. 4 it is shown that the elastic scattering dominates the total mean free path, mostly at low energies.

In Fig. 5 we represent for different electron excitation energies, the angular distribution of excited electrons $S(v;\varepsilon,\Omega)$ for projectiles traveling through a free electron gas ($r_s=1.5$ a.u.) with velocity $v=0.6$ a.u. Figure 5(a) corresponds to $Z_1=1$ projectile and Fig. 5(b) to $Z_1=10$. These distributions are strongly anisotropic and peaked in the di-

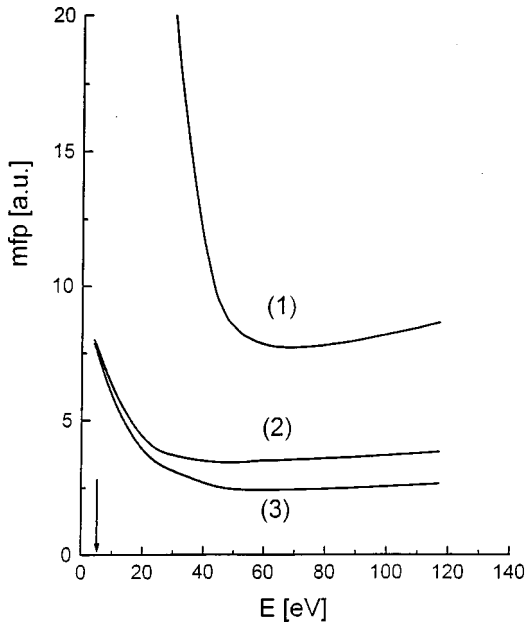

FIG. 4. Calculated mean free path (MFP) of electrons in Au as a function of the electron energy (measured from the Fermi level). (1), (2), and (3) denote the inelastic, elastic, and the total MFP, respectively. The vacuum level is indicated by an arrow in the figure.

rection of the velocity of the projectile. For ions in normal incidence it means that the majority of the excited electrons are excited in the direction opposite to the entrance surface.

When the elastic scattering is considered the density of inner excited electrons $N(\varepsilon,\Omega)$ becomes nearly isotropic.[20] Therefore, in the backward direction $N(\varepsilon,\Omega)$ is enlarged by elastic scattering, producing an enhancement of the backward emission yield.

In Fig. 6 the backward emission yield γ induced by hydrogen projectiles in normal incidence on Au calculated neglecting and including the elastic scattering is presented as a function of the velocity of the ion. As anticipated above, the total electron yield is much larger when the elastic scattering is considered. This effect is seen to be more pronounced with decreasing ion velocity. This can be easily understood since the energy range of excited electrons is shifted to lower energies when decreasing ion velocity $[\varepsilon_{\max}=2v(v+v_F)]$ and the elastic scattering effect is more important at low energies (see Fig. 4).

B. H and He projectiles

For H and He projectiles at low velocities, the excitation mechanism calculated here, i.e., the creation of electron-hole pairs in the conduction band of the metal, is the main mechanism that contributes to the kinetic electron emission. In Figs. 7 and 8, the backward emission yields γ calculated with both the model presented here and the model of Ref. 6 are compared to experimental data obtained by different groups[25,26,27,28] as a function of the velocity of the projectile, for H and He ions in normal incidence on Au.

Both theoretical models give similar results, though as anticipated before, the yields are always higher when the shift of the Fermi sphere is taken into account, as in this model either more primary electrons are excited above the

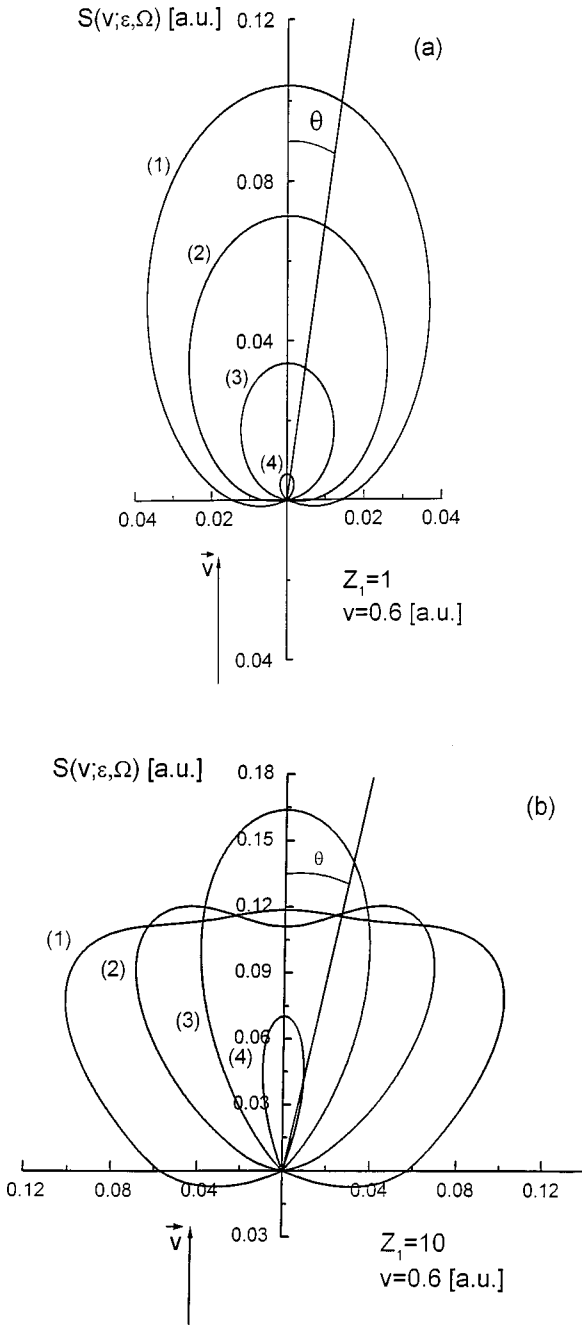

FIG. 5. Angular distributions of electrons $S(v;\varepsilon,\Omega)$ at different excitation energies ε in an electron gas with $r_s=1.5$ a.u., for $v=0.6$ a.u. projectiles as a function of θ, the angle between the velocity of the excited electron and the projectile velocity. In (a) the atomic number of the projectile is $Z_1=1$ and in (b) $Z_1=10$. The excitation energies ε related to (1), (2), (3), and (4) are 10, 15, 25, and 45 eV for $Z_1=1$ and 10, 25, 45, and 57 eV for $Z_1=10$, respectively. All energies are measured from the Fermi level. The distance to the center corresponds to the value of the excitation function in a.u.

work function of the metal or as the primary electrons are excited at higher energies, in the decay process regulated by the second term on the right-hand side of Eq. (27) more secondary electrons are excited. The agreement between experimental and theoretical results is quite satisfactory.

In Fig. 7 it is also shown for comparison the backward emission yield for a proton projectile, when the electronic

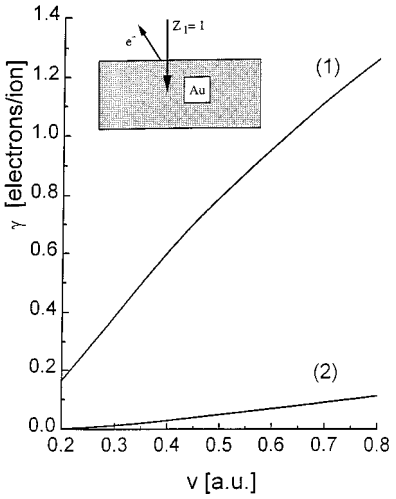

FIG. 6. Effect of elastic scattering. Projectile velocity dependence of the backward yield for proton impact on Au. (1) and (2) denote the yield with and without including elastic scattering in the transport process.

excitation is obtained calculating the potential induced by the projectile within linear response theory and the electron scattering in first born approximation.[29] The dielectric function used has been obtained in the random phase approximation.[21] The results show that this approach is not valid at these low ion velocities since it gives too small values for the yield of emitted electrons. This is consistent with the results obtained in the calculations of the stopping power of slow protons in an electron gas.[16]

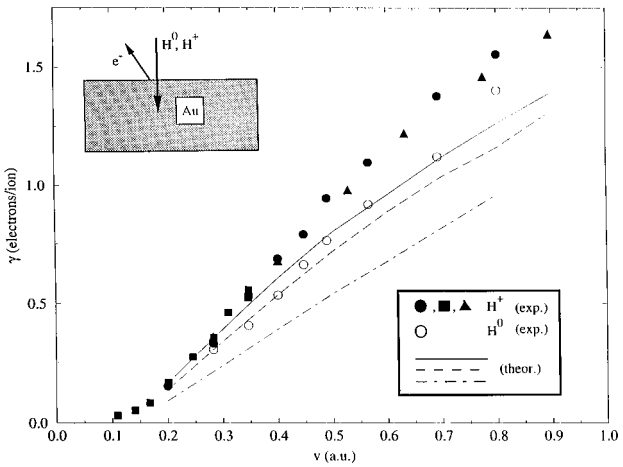

FIG. 7. Comparison between the theoretical results and experimental data of the backward kinetic electron yield induced by a hydrogen atom in normal incidence on a clean Au surface as a function of the velocity of the projectile. Solid line is the result obtained using the model presented in this work. Dashed line is obtained with the excitation function given in Ref. 6. The experimental data are as follows: open circles correspond to H^0 projectiles from Ref. 26, full circles to H^+ projectiles from Ref. 26, full triangles to H^+ projectiles from Ref. 25, and full squares to H^+ projectiles from Ref. 27. The dashed-dotted line represents the results obtained when the excitation induced by a proton is calculated making use of the dielectric formalism. In the theoretical calculations $r_s = 1.5$ a.u. has been used.

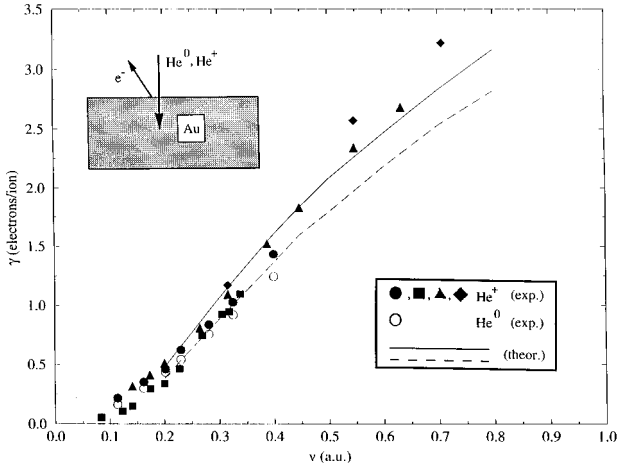

FIG. 8. Comparison between the theoretical results and experimental data of the backward kinetic electron yield induced by a helium atom in normal incidence on a clean Au surface as a function of the velocity of the projectile. The solid line is the result obtained using the model presented in this work. The dashed line is obtained with the excitation function given in Ref. 6. The experimental data are as follows: open circles correspond to He^0 projectiles from Ref. 26, full circles to He^+ projectiles from Ref. 26, full triangles to He^+ projectiles from Ref. 25, full squares to He^+ projectiles from Ref. 27, and full diamonds to He^+ projectiles from Ref. 28. In the theoretical calculations $r_s = 1.5$ a.u. has been used.

The experimental yields are higher for H^+ and He^+ than for neutral H^0 and He^0. This difference was explained by Lakits *et al.*[30] with a model which used the larger value of the stopping power of the singly charged ions compared to the stopping power of the neutral particles and the neutralization rates of the singly charged ions. Our theoretical results are obtained for the equilibrium configurations of the DFT formalism, hence we expect that our calculation is more suitable for the neutral particles. Anyway, study of the dependence of kinetic electron yield on the charge state of the projectile is beyond the scope of this work.

It is noticeable that the largest difference between the experimental data and the theoretical results appears at high projectile velocities where the theoretical models underestimate the total yield. This was an expected result, and the reason was discussed in the previous section. On the one hand, in the model of Ref. 6, the underestimation of the number of electrons excited over the work function of the metal increases with the velocity. And, on the other hand, when the shift of the Fermi sphere is taken into account, the reduction of the excitation due to the use of the static potential instead of the dynamic potential is also more important when increasing the velocity of the projectile.

C. Z_1 dependence of the electron yield

In Fig. 9 the calculated total backward kinetic electron yield for 20 keV projectiles ($Z_1 = 1-19$) in normal incidence on Au is compared to available experimental data.[31–33,25] In this case, some important differences are found between the experimental data and the theoretical results. Probably, besides the mechanism consisting on electron-hole pair formation in the conduction band of the

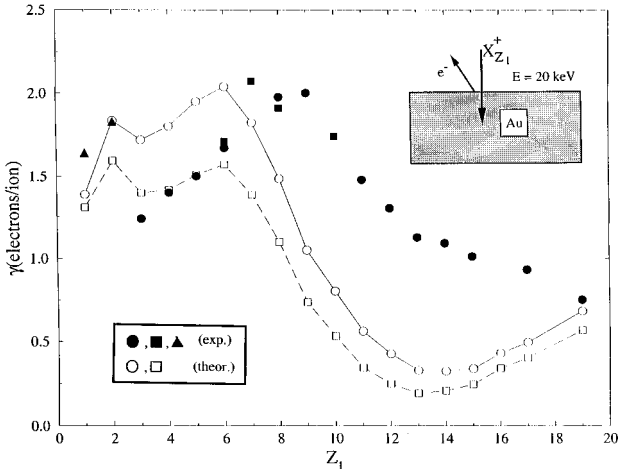

FIG. 9. Backward kinetic electron yield induced by 20 keV ions in normal incidence on Au as a function of the projectile atomic number Z_1. The open circles are the results obtained using the model presented in this work and open squares with the excitation function given in Ref. 6. The solid and dashed lines are used to guide the eye. The full circles are experimental data from Ref. 31, the triangles are experimental data from Ref. 25, and the full squares are experimental data from Refs. 32 and 33. In the theoretical calculations $r_s = 1.5$ a.u. has been used.

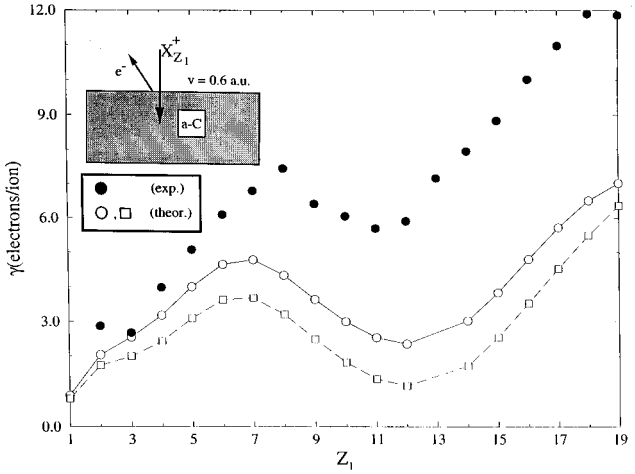

FIG. 10. Backward kinetic electron yield induced by ion projectiles with velocity $v = 0.6$ a.u. in normal incidence on amorphous carbon as a function of Z_1 the atomic number of the projectile. The open circles are obtained using the excitation function calculated using the model presented in this work, and open squares with the excitation function calculated as in Ref. 6. The solid and dashed lines are used to guide the eye. The full circles correspond to the experimental data from Ref. 39. In the theoretical calculations $r_s = 1.66$ a.u. has been used.

metal that has been considered here, additional electronic excitation is taking place due to other mechanisms as electron excitation by recoiled target atoms[2,34] and emission of electrons bound to the projectile and target atoms via electron promotion when molecular orbitals are created in close collisions between projectiles and target atoms.[35–37] The existence of these other mechanisms can explain the higher experimental yield compared to the theoretical results for $Z_1 = 7-19$. In particular, the dependence of the electron promotion mechanism on both projectile and target atomic numbers could explain[38] the different position of the theoretical and experimental yield maximum. Anyway, it is observed that the contribution of electron-hole pair creation mechanism is not negligible at this projectile energy and in this range of atomic numbers.

In the case of $Z_1 = 3-6$, the order of magnitude of the experimental yields and the experimentally found increasing behavior of the yield with Z_1 is obtained in the calculated results, but the fact that the theoretical yields are larger than the experimental ones can only be explained by the limitations of the model related to the difficulties in the calculation of the elastic scattering properties and the free electron-gas approximation.

Finally, in Fig. 10 the theoretical results obtained for the backward electron yield and the experimental data[39] at constant projectile velocity ($v = 0.6$ a.u.) are compared, as a function of Z_1 the atomic number of the projectile. The target material is amorphous carbon, and a value of $r_s = 1.66$ a.u. has been used to represent its conduction band.[24] The elastic scattering properties are determined within a model of randomly distributed atoms using the partial wave expansion method. The phase shifts for carbon are calculated with an atomic potential given by Bonham and Strand.[40] In this case, a good approximation is obtained for the position of the maxima and the minima. It suggests that for this higher velocity ions, the relative contribution of the electron promotion mechanism is less important than for the lower velocity ions of Fig. 9, where it can change the position of the maxima and minima that our model gives. In any case, the experimental yields are somewhat higher than the theoretical results, and the difference between them increases with the atomic number of the projectile, suggesting additional electron excitation induced by recoiling target atoms.[34]

The discrepancies between the theory and experiment for slow Z_1 ions, have also been observed in the stopping power by Echenique *et al.*[41] using the DFT theory for a homogeneous electron gas. Extending the calculation to nonhomogeneous electron distributions, and including in an effective way the valence and core electrons Calera-Rubio *et al.*[42] obtained good agreement with the experimental stopping power data.

IV. CONCLUSION

In this work a model has been presented to calculate the kinetic electron emission induced by slow ions in metals. The shift of the Fermi sphere has been taken into account and a nonlinear calculation of the perturbation created by the projectile and of the scattering suffered by the electrons has been performed in order to calculate the angle and energy distribution of the primary excited electrons. Using this excitation function and solving the transport equation total electron yields are calculated. The strong influence of the elastic scattering of the excited electrons on the backward electron yield has been analyzed.

Good agreement has been obtained for the backward yield induced by light projectiles such as H and He, between the theoretical results and the experimental data. It is noticeable, that a simplified and less realistic method in which the shift of the Fermi sphere was not taken into account, gives also

similar results for the total yields. This indicates that the model of Ref. 6 is a good approximation to calculate total yields. Anyway, it is not valid to calculate energy distributions of emitted electrons as the maximum excitation energy is not properly calculated within this model.

For high Z_1 ions, larger differences are observed between our theoretical results and the experiments. These differences come mostly because in the case of high Z_1 ions, another electron excitation mechanisms as electron promotion via formation of molecular orbitals and electron excitation by recoiling target atoms may be playing a role. Nevertheless, it is observed that conduction band electron excitation is an efficient electron ejection mechanism in the range of velocities and atomic number of projectiles studied.

ACKNOWLEDGMENTS

We are indebted to Hannes Eder for providing us with the unpublished experimental data for the electron emission induced by 20 keV C^+, O^+, and Ne^+ ions in Au. We are grateful to Andrés Arnau for helpful discussions. J.I.J. and F.J.G.A. acknowledge help and support from Eusko Jaurlaritza/Gobierno Vasco, Universidad del País Vasco/Euskal Herriko Unibertsitatea, Ministerio de Educación y Cultura (Project No. PB92-0474) and Iberdrola S. A.

[1] H. D. Hagstrum, Phys. Rev. **96**, 325 (1954); **96**, 336 (1954).
[2] E. J. Sternglass, Phys. Rev. **108**, 1 (1957).
[3] J. Schou, Phys. Rev. B **22**, 2141 (1980).
[4] P. M. Echenique, F. Flores, and R. H. Ritchie, in *Solid State Physics: Research and Applications*, edited by H. Ehrenreich and D. Turnbull (Academic, New York, 1990), Vol. 43, p. 229.
[5] J. I. Juaristi, M. Rösler, F. J. García de Abajo, H. Kerkow, and R. Stolle, Nucl. Instrum. Methods Phys. Res. B **135**, 487 (1998).
[6] J. Calera-Rubio, A. Gras-Martí, N. R. Arista, M. M. Jakas, Z. Sroubek, and G. Falcone, Surf. Sci. **251/252**, 136 (1989).
[7] J. Calera-Rubio, A. Gras-Martí, N. R. Arista, M. M. Jakas, Z. Sroubek, and G. Falcone, Radiat. Eff. Defects Solids **117**, 173 (1991).
[8] L. T. Schiff, *Quantum Mechanics* (McGraw-Hill, New York, 1985).
[9] A. Mazarro, P. M. Echenique, and R. H. Ritchie, Phys. Rev. B **27**, 4117 (1983).
[10] P. Hohenberg and W. Kohn, Phys. Rev. **136**, B864 (1964).
[11] W. Kohn and L. J. Sham, Phys. Rev. **140**, A1133 (1965).
[12] E. Zaremba, L. M. Sander, H. B. Shore, and J. H. Rose, J. Phys. F **7**, 1763 (1977).
[13] E. W. McDaniel, *Atomic Collisions; Electron and Photon Projectiles* (Wiley, New York, 1989).
[14] G. Falcone and Z. Sroubek, Phys. Rev. B **39**, 1999 (1989).
[15] T. L. Ferrell and R. H. Ritchie, Phys. Rev. B **16**, 115 (1977).
[16] P. M. Echenique, R. M. Nieminem, and R. H. Ritchie, Solid State Commun. **37**, 7791 (1981).
[17] A. Mann and W. Brandt, Phys. Rev. B **24**, 4999 (1981).
[18] P. M. Echenique, F. J. García de Abajo, V. H. Ponce, and M. E. Uranga, Nucl. Instrum. Methods Phys. Res. B **96**, 583 (1995).
[19] E. Zaremba, A. Arnau, and P. M. Echenique, Nucl. Instrum. Methods Phys. Res. B **96**, 619 (1995).
[20] M. Rösler and W. Brauer, in *Particle Induced Electron Emission I*, edited by G. Höhler, Vol. 122 of Springer Tracts in Modern Physics (Springer, Berlin, 1991).
[21] J. Lindhard, K. Dan. Vidensk. Selsk. Mat. Fys. Medd. **28**, 8 (1954).
[22] K. Heinz (private communication).
[23] C. C. Ahn, O. L. Krivanek, R. P. Buerger, M. M. Disko, and P. R. Swan, *Electron Energy Loss Spectroscopy Atlas* (Gatan, Warrendale, PA, 1983).
[24] D. Isaacson, New York University Document No. 02698 (National Auxiliary Publication Service, New York, 1975).
[25] R. A. Baragiola, E. V. Alonso, and A. Oliva Florio, Phys. Rev. B **19**, 121 (1979).
[26] G. Lakits and HP. Winter, Nucl. Instrum. Methods Phys. Res. B **48**, 597 (1990).
[27] H. Eder, M. Vana, F. Aumayr, and HP. Winter, Rev. Sci. Instrum. **68** (1), 165 (1997).
[28] J. Ferrón, E. V. Alonso, R. A. Baragiola, and A. Oliva Florio, Phys. Rev. B **24**, 4412 (1984).
[29] R. H. Ritchie, Phys. Rev. **114**, 644 (1959).
[30] G. Lakits, A. Arnau, and HP. Winter, Phys. Rev. B **42**, 15 (1990).
[31] F. Thum and W. O. Hofer, Nucl. Instrum. Methods Phys. Res. B **2**, 531 (1984).
[32] H. Eder (private communication).
[33] H. Eder, M. Vana, F. Aumayr, HP. Winter, J. I. Juaristi, and A. Arnau, Phys. Scr. **T73**, 322 (1997).
[34] G. Holmen, B. Svensson, J. Schou, and P. Sigmund, Phys. Rev. B **20**, 2247 (1979).
[35] E. S. Parilis and L. M. Kishineskii, Fiz. Tverd. Tela (Leningrad) **3**, 1219 (1960) [Sov. Phys. Solid State **3**, 885 (1960)].
[36] W. Weisel and O. Beck, Z. Phys. **76**, 250 (1932).
[37] U. Fano and W. Lichten, Phys. Rev. Lett. **14**, 627 (1950).
[38] M. M. Ferguson and W. O. Hofer, Radiat. Eff. Defects Solids **109**, 273 (1989).
[39] St. Gelfort, H. Kerkow, R. Stolle, V. P. Petukohv, and E. A. Romanovskii, Nucl. Instrum. Methods Phys. Res. B **125**, 49 (1997).
[40] R. Bonham and T. G. Strand, J. Chem. Phys. **39**, 2200 (1963).
[41] P. M. Echenique, R. M. Nieminem, J. C. Ashley, and R. H. Ritchie, Phys. Rev. A **33**, 897 (1986).
[42] J. Calera-Rubio, A. Gras-Martí, and N. R. Arista, Nucl. Instrum. Methods Phys. Res. B **93**, 137 (1994).